TRENDS IN SCIENCES 2026; 23(10): 13199
https://doi.org/10.48048/tis.2026.13199 RESEARCH ARTICLE

# Green Synthesis of Silver Nanoparticles Using *Syzygium gratum* Branch Extract: Physicochemical Characterization, and Antibacterial Activities

**Amornrassamee Jinnarak[1], Taweesub Juepanit[1], Nichanun Udomsaksakul[2], Wuttichai Roschat[3,4] and Phakawan Kongchantree[1,*]**

[1]*Department of Chemistry, Faculty of Science and Technology, Rajabhat Rajanagarindra University, Chachoengsao 24000, Thailand*
[2]*Department of Applied Biology, Faculty of Science and Technology, Rajabhat Rajanagarindra University, Chachoengsao 24000, Thailand*
[3] *Biomass Energy Research Laboratory, Center of Excellence on Alternative Energy, Research and Development Institution, Sakon Nakhon Rajabhat University, Sakon Nakhon 47000, Thailand*
[4]*Program of Chemistry, Faculty of Science and Technology, Sakon Nakhon Rajabhat University, Sakon Nakhon 47000, Thailand*

**([*]Corresponding author's e-mail: tassawan.kon@rru.ac.th)**

*Received: 30 December 2025, Revised: 26 January 2026, Accepted: 15 February 2026, Published: 20 April 2026*

**Abstract**

Green synthesis offers a sustainable alternative for producing metal nanoparticles with controlled structural and functional properties. In this study, silver nanoparticles (AgNPs) were successfully synthesized using *Syzygium gratum* branch extract as a natural reducing and stabilizing agent. The formation of AgNPs was confirmed by the emergence of a characteristic surface plasmon resonance band at 436 nm. Systematic optimization of reaction parameters, including silver nitrate concentration, extract volume, and incubation time, enabled reproducible nanoparticle formation under ambient conditions. Comprehensive physicochemical characterization using UV–Vis spectroscopy, FT-IR, XRD, SEM, HRTEM, EDX, dynamic light scattering, and zeta-potential analysis revealed the formation of crystalline silver nanostructures with a face-centered cubic lattice. XRD analysis indicated an average crystallite size of 11.64 nm, while electron microscopy showed predominantly quasi-spherical nanoparticles with sizes ranging from 2 to 50 nm. The hydrodynamic particle size was 66.64 nm with a polydispersity index of 0.239, and a negative zeta potential value of −35 mV demonstrated good colloidal stability. FT-IR spectral shifts associated with hydroxyl, carbonyl/amide, and C–O functional groups confirmed the involvement of plant-derived phytochemicals in silver ion reduction and nanoparticle surface capping. The biosynthesized AgNPs exhibited pronounced antibacterial activity against both Gram-positive and Gram-negative bacterial strains. At a concentration of 10 mM, inhibition zones ranging from 12.67 ± 1.15 to 18.67 ± 0.58 mm were observed, with statistically significant differences ($p < 0.05$) for five of the six tested strains. The enhanced antibacterial performance is attributed to the small particle size, high surface area, and stable dispersion of the AgNPs. Therefore, this work demonstrates that *Syzygium gratum* branch extract effectively governs nanoparticle nucleation, growth, and stabilization. The proposed environmentally benign synthesis route provides a reproducible strategy for producing functional silver nanomaterials with potential applications in antimicrobial and biointerface-related fields.

**Keywords:** Green synthesis, Silver nanoparticles, *Syzygium gratum*, Antibacterial activity, Physicochemical characterization

**Introduction**

Metal nanoparticles have garnered considerable attention due to their distinctive characteristics, including large surface area, high physical stability, tunable synthesis routes, and ease of surface modification [1,2]. These features endow them with remarkable electrical, optical, and catalytic properties, making them attractive for diverse applications such as permeability enhancement and functional fillers. Among noble-metal–based nanomaterials, gold (Au)– and silver (Ag)–containing nanostructures have attracted considerable attention owing to their ability to tailor the structural, optical, and functional properties of advanced materials, particularly in polymeric and glass-based systems for radiation-related and optoelectronic applications [3,4]. Nevertheless, silver nanoparticles (AgNPs) have received greater emphasis in both industrial applications and fundamental research due to their outstanding performance in catalysis, sensing, gas adsorption, antioxidant activity, medical applications, and antibacterial effects [5-9]. Various physical and chemical techniques have been employed for AgNPs synthesis, including solution-phase reduction [10], thermal decomposition of silver compounds [11], microwave-assisted methods [12], high-energy irradiation [13], photocatalytic processes [14], and mechanical milling [15]. Among these, chemical reduction remains the most widely adopted approach, utilizing organic or inorganic reducing agents such as hydrazine [16], ascorbic acid [17], sodium borohydride [18], and polyethylene glycol [19]. These reducing and capping agents play a crucial role in controlling the size and morphology of AgNPs by converting Ag(I) ions into metallic Ag (0) in aqueous or non-aqueous systems [20].

Despite their effectiveness, conventional physical and chemical synthesis routes are often associated with high costs due to the requirement for elevated temperatures, high pressures, complex instrumentation, and substantial energy consumption. In addition, these methods frequently generate toxic by-products that pose environmental and biological safety concerns [21,22]. Consequently, the development of sustainable and environmentally benign nanoparticle synthesis strategies has become increasingly important, in line with the growing emphasis on green chemistry and eco-friendly technologies [23]. The integration of green chemistry principles into nanoparticle production not only minimizes environmental impact but also aligns with sustainable industrial practices [24,25]. Green synthesis approaches exploit natural resources such as microorganisms, enzymes, plant extracts, and biodegradable materials as reducing and stabilizing agents for nanoparticle fabrication [26]. In particular, plant-mediated synthesis offers distinct advantages, including simplicity, scalability, and the ability to produce nanoparticles with controlled size and morphology. However, most reported plant-mediated AgNP synthesis studies primarily focus on leaf extracts, with limited attention given to woody plant tissues and their unique phytochemical environments. As a result, the influence of tissue-specific phytochemical composition—particularly that of lignified and tannin-rich woody organs—on nanoparticle surface chemistry and functional performance remains insufficiently explored.

*Syzygium gratum* (Wight) S.N. Mitra var. *gratum*, belonging to the family Myrtaceae, is a plant that grows well under a wide range of soil conditions throughout Thailand. It is commonly consumed as a fresh or blanched vegetable, prepared as herbal tea, or finely ground and applied topically to reduce bruising [27]. The plant is widely distributed across the country and has long been recognized as an ethnomedicinal species for the treatment of cuts and wounds. Traditionally, its leaves have been used to alleviate dysentery, indigestion, and gastrointestinal disorders [28]. Previous phytochemical investigations have demonstrated that *Syzygium* leaf extracts are rich in phenolic compounds, including flavonoids and other secondary metabolites with pronounced biological activity [29]. In contrast to leaf tissues, woody organs such as branches represent a distinct phytochemical matrix characterized by higher proportions of condensed tannins, polymeric phenolics, and lignin-associated compounds. These components are expected to alter the reduction–stabilization balance during green nanoparticle synthesis and to imprint a unique surface-associated chemical identity onto the resulting nanoparticles. To the best of our knowledge, the utilization of *Syzygium gratum* branch extract for the green synthesis of silver nanoparticles, with an emphasis on understanding how a woody-tissue-derived phytochemical environment governs nanoparticle

surface chemistry and antibacterial performance, has not been previously reported. Accordingly, *Syzygium gratum* branch extract was selected in this study not with the primary aim of optimizing nanoparticle yield or size, but rather to systematically examine how tissue-specific phytochemical context influences AgNP formation, surface functionalization, and biological activity under controlled synthesis conditions.

Plant-derived phytoconstituents—including proteins, alkaloids, saponins, terpenoids, flavonoids, tannins, phenols, and polyphenols—have been consistently reported to participate in metal-ion reduction and nanoparticle stabilization through surface coordination and capping interactions during green synthesis [30]. The intrinsic redox activity of these metabolites facilitates the formation of metallic nanoparticles while contributing to colloidal stabilization [31,32]. Accordingly, plant-mediated nanoparticle synthesis is widely regarded as an environmentally benign and operationally straightforward approach for generating functional nanomaterials without reliance on harsh chemical reagents or complex post-synthetic processing.

In the present study, *Syzygium gratum* branch extract was employed as a biogenic reducing and stabilizing agent for the conversion of silver nitrate into silver nanoparticles. Unlike most previous green synthesis studies that predominantly utilize leaf-derived extracts, this work specifically exploits woody-tissue-derived phytochemical matrices to elucidate their role in encoding surface-associated chemical identity onto AgNPs. The synthesized AgNPs were systematically characterized using UV–visible spectroscopy, Fourier transform infrared spectroscopy (FTIR), X-ray diffraction (XRD), field-emission scanning electron microscopy (SEM), energy-dispersive X-ray spectroscopy (EDX), high-resolution transmission electron microscopy (HRTEM), and zeta potential analysis. This integrated characterization approach enables direct correlation between phytochemical-mediated nanoparticle nucleation, growth behavior, surface chemistry, and colloidal stability. Furthermore, the antibacterial efficacy of the branch-derived, phytochemically encoded AgNPs was evaluated against six clinically relevant pathogenic bacterial strains, namely *Pseudomonas aeruginosa* (*P. aeruginosa*), *Listeria monocytogenes* (*L. monocytogenes*), *Escherichia coli* (*E. coli*), *Staphylococcus aureus* (*S. aureus*), *Salmonella typhimurium* (*S. typhimurium*), and *Bacillus cereus* (*B. cereus*). By linking surface chemical identity to antibacterial performance, this study provides mechanistic insight that extends beyond conventional reports of green nanoparticle synthesis.

## Materials and methods

### Materials

Silver nitrate ($AgNO_3$, ≥ 99%) was purchased from Merck. Fresh branches of *Syzygium gratum* were purchased from a local market in Thailand. The bacterial strains *E. coli*, *P. aeruginosa*, *S. aureus*, *L. monocytogenes*, *S. typhimurium*, and *B. cereus* were sourced from the American Type Culture Collection (ATCC, Manassas, VA, USA). All chemicals used in this study were of analytical reagent grade and were employed without further purification.

### *Syzygium gratum* branch extract preparation

Fresh small branches of *Syzygium gratum* were collected and thoroughly washed with distilled water two to three times to remove surface impurities. The cleaned branches were shade-dried for 30 min, chopped into small pieces using scissors, and subsequently dried in a hot-air oven for 1 h. The dried material was then ground into a fine powder using a blender. A total of 20 g of the powdered branches was mixed with 500 mL of distilled water and heated at 100 °C for 1 h under continuous magnetic stirring. After cooling to room temperature, the mixture was filtered through Whatman No. 1 filter paper. The resulting filtrate was collected and stored at 4 °C for further use. The prepared branch extract was employed as a green reducing and capping agent for the biosynthesis of silver nanoparticles (AgNPs). The extraction conditions were selected to preserve thermally sensitive phenolic and polyphenolic compounds while ensuring sufficient extraction efficiency for reducing and stabilizing agents.

### Optimization of green synthesis of AgNPs

In this study, the standard reaction system for the green synthesis of silver nanoparticles consisted of 250 µL of *Syzygium gratum* branch extract mixed with 25 mL of an aqueous $AgNO_3$ solution at a concentration of 10 mM. The reaction mixture was continuously

stirred using a magnetic stirrer at room temperature for 30 min to ensure homogeneous interaction between the plant extract and silver ions. This condition was selected as the baseline for subsequent optimization experiments. To evaluate the effect of silver precursor concentration, the $AgNO_3$ concentration was systematically varied in the range of 0.25 - 50 mM while maintaining a constant extract volume. The branch extract alone and a 10 mM $AgNO_3$ solution without extract were used as control samples to distinguish bioreduction-induced nanoparticle formation from background effects. The influence of extract concentration was examined by varying the volume of branch extract from 50 to 500 µL, with the total reaction volume adjusted accordingly to maintain the $AgNO_3$ concentration at 10 mM. In addition, the effect of reaction time on nanoparticle formation was investigated by incubating the optimized reaction mixture for periods ranging from 30 min to 240 h. These parameters were selected based on preliminary trials and literature-reported green synthesis conditions to balance nucleation rate, particle growth, and colloidal stability. The progress of AgNPs formation under all experimental conditions was monitored by recording the UV–Vis absorption spectra of the reaction solutions, with particular attention to the evolution of the surface plasmon resonance band characteristic of silver nanoparticles. The stepwise synthesis process and the underlying reduction and stabilization mechanisms involved in AgNPs formation are schematically illustrated in **Scheme 1**, which presents the proposed mechanism for the green synthesis of silver nanoparticles (AgNPs) mediated by *Syzygium gratum* branch extract.

**Characterization of synthesized silver nanoparticles**

The optical properties of the synthesized silver nanoparticles (AgNPs) were analyzed using a UV–visible spectrophotometer (GENESYS 50 UV–Vis) over a suitable wavelength range, with a spectral resolution of 0.5 nm. The morphology, size, and elemental composition of the AgNPs were examined using scanning electron microscopy (SEM) and energy-dispersive X-ray spectroscopy (EDX). For SEM and EDX analyses, the reaction mixture was dried and analyzed using a JEOL JEM-3100F instrument operated at an accelerating voltage of 300 kV. The detailed morphology and crystalline features of the nanoparticles were further investigated by high-resolution transmission electron microscopy (HRTEM). For HRTEM analysis, a drop of the aqueous AgNP suspension was deposited onto a carbon-coated copper grid and allowed to dry at ambient conditions. TEM micrographs and selected-area electron diffraction (SAED) patterns were recorded using a Hitachi HT7700 transmission electron microscope operated at 200 kV. The average particle size and size distribution of the AgNPs were determined using a particle size analyzer (Zetasizer Nano ZS, Malvern Instruments). The crystalline structure of the AgNPs was characterized by X-ray diffraction (XRD) using Cu Kα radiation (λ = 1.5406 Å). The XRD measurements were performed at an operating voltage of 40 kV and a current of 40 mA, with continuous scanning over a 2θ range of 4° - 90°. Functional groups associated with the biomolecules involved in nanoparticle synthesis were identified using Fourier transform infrared (FTIR) spectroscopy (Nicolet iN10, USA) employing the KBr pellet technique. FTIR spectra were recorded in transmission mode over 50 scans at a resolution of 4 $cm^{-1}$. In addition, the hydrodynamic particle size distribution and surface charge (zeta potential) of the AgNPs were measured using a Zetasizer Nano ZS (Malvern Instruments) at 25 °C with a detection angle of 90°.

**Antibacterial activity of synthesized silver nanoparticles**

The antibacterial activity of the synthesized silver nanoparticles (AgNPs) was evaluated in triplicate against representative Gram-positive and Gram-negative bacterial strains, including *E. coli*, *P. aeruginosa*, *S. aureus*, *L. monocytogenes*, *S. typhimurium*, and *B. cereus*. The selected bacterial strains represent both Gram-positive and Gram-negative pathogens commonly associated with clinical and environmental infections, enabling a broad evaluation of antibacterial efficacy. The antibacterial efficacy of the AgNPs was assessed using the disk diffusion method. Briefly, bacterial suspensions were adjusted to 0.5 McFarland standard and uniformly spread onto the surface of Mueller–Hinton agar plates. Sterile disks impregnated with 50 µL of the AgNP sample were placed onto the inoculated agar surfaces, followed by incubation at 35 °C for 24 h. After incubation, the plates

were examined for the presence of inhibition zones, indicated by clear areas surrounding the disks. The diameters of the zones of inhibition were measured in millimeters, and the mean values for each bacterial strain were calculated from three independent replicates.

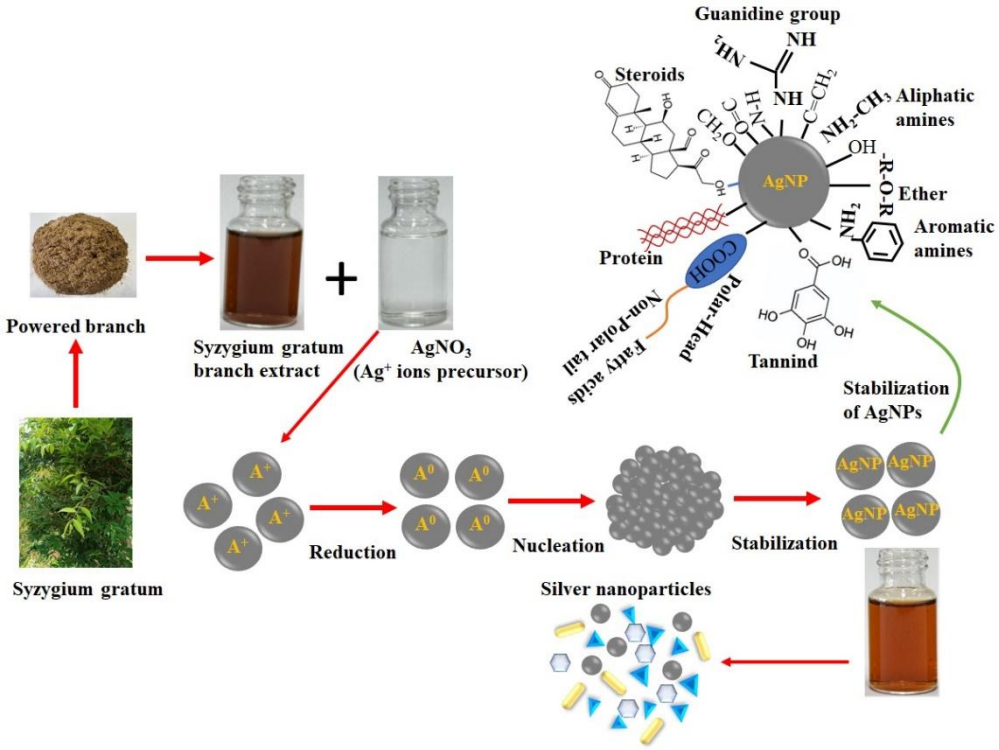


**Scheme 1** Proposed mechanism for the green synthesis of silver nanoparticles (AgNPs) mediated by *Syzygium gratum* branch extract.

## Results and discussion

### UV–Vis spectroscopy analysis

The biosynthesis of silver nanoparticles (AgNPs) using *Syzygium gratum* branch extract was systematically investigated using UV–visible spectroscopy. Noble metal nanoparticles such as silver exhibit distinctive optical properties arising from surface plasmon resonance (SPR), which originates from the collective oscillation of conduction-band electrons upon interaction with incident light [33]. During the reduction process, a visible color change from pale yellow to reddish brown was observed, providing a preliminary indication of AgNP formation. The observed color variation was consistent with the surface plasmon resonance (SPR) absorption band, a distinctive optical feature of metallic silver nanoparticles. This finding is in good agreement with previously reported studies by Sun *et al*. [34] and Pugazhenthiran *et al*. [35], which similarly attributed such color changes to the SPR behavior of silver nanoparticles.

The absorption spectra revealed a narrow and well-defined SPR peak centered at 436 nm, confirming the formation of stable and monodispersed AgNPs (**Figure 1(a)**). This SPR band, arising from collective electron oscillations on the nanoparticle surface, is commonly employed as a reliable indicator for monitoring AgNP synthesis and stability [36,37]. Continuous spectral monitoring at regular time intervals confirmed the efficient and sustained formation of AgNPs, as evidenced by the progressive evolution of the characteristic surface plasmon resonance band. These observations are in close agreement with earlier studies by Bazrgaran *et al*. [38] and Priyadarshini *et al*. [39], who reported similar time-dependent spectral behavior during plant-mediated synthesis of silver nanoparticles, attributing it to the gradual reduction of $Ag^+$ ions and stabilization of the resulting nanoparticles by phytochemical constituents. The phytochemicals

present in the *Syzygium gratum* branch extract acted simultaneously as reducing, capping, and stabilizing agents. Phytochemical screening confirmed the presence of alkaloids, saponins, tannins, phenols, anthraquinones, flavonoids, glycosides, and polyphenols, which are known to facilitate the reduction of $Ag^+$ ions to $Ag^0$ and stabilize the resulting nanoparticles. A proposed mechanism illustrating $Ag^+$ reduction and nanoparticle stabilization is presented in **Scheme 1**.

The effect of the branch extract-to-silver nitrate ratio on AgNP formation is illustrated in **Figure 1(b)**. Reaction mixtures containing 50 - 500 µL of *Syzygium gratum* branch extract were examined while maintaining a constant $AgNO_3$ concentration. A gradual color transition from pale yellow to reddish brown was observed across this range, indicating nanoparticle formation. Among the tested conditions, 250 µL of branch extract produced the most intense and narrow SPR peak, suggesting the formation of smaller and more stable AgNPs [40]. In contrast, extract volumes exceeding 250 µL resulted in broader SPR bands with reduced intensity, implying decreased nanoparticle stability and possible aggregation. Similar effects have been reported for nanoparticle synthesis mediated by plant bark and leaf extracts [41,42]. At higher extract concentrations, the excess biomolecules may hinder effective silver ion reduction, leading to reduced nanoparticle formation [43,44]. Consequently, 250 µL of branch extract was selected as the optimal volume for subsequent experiments.

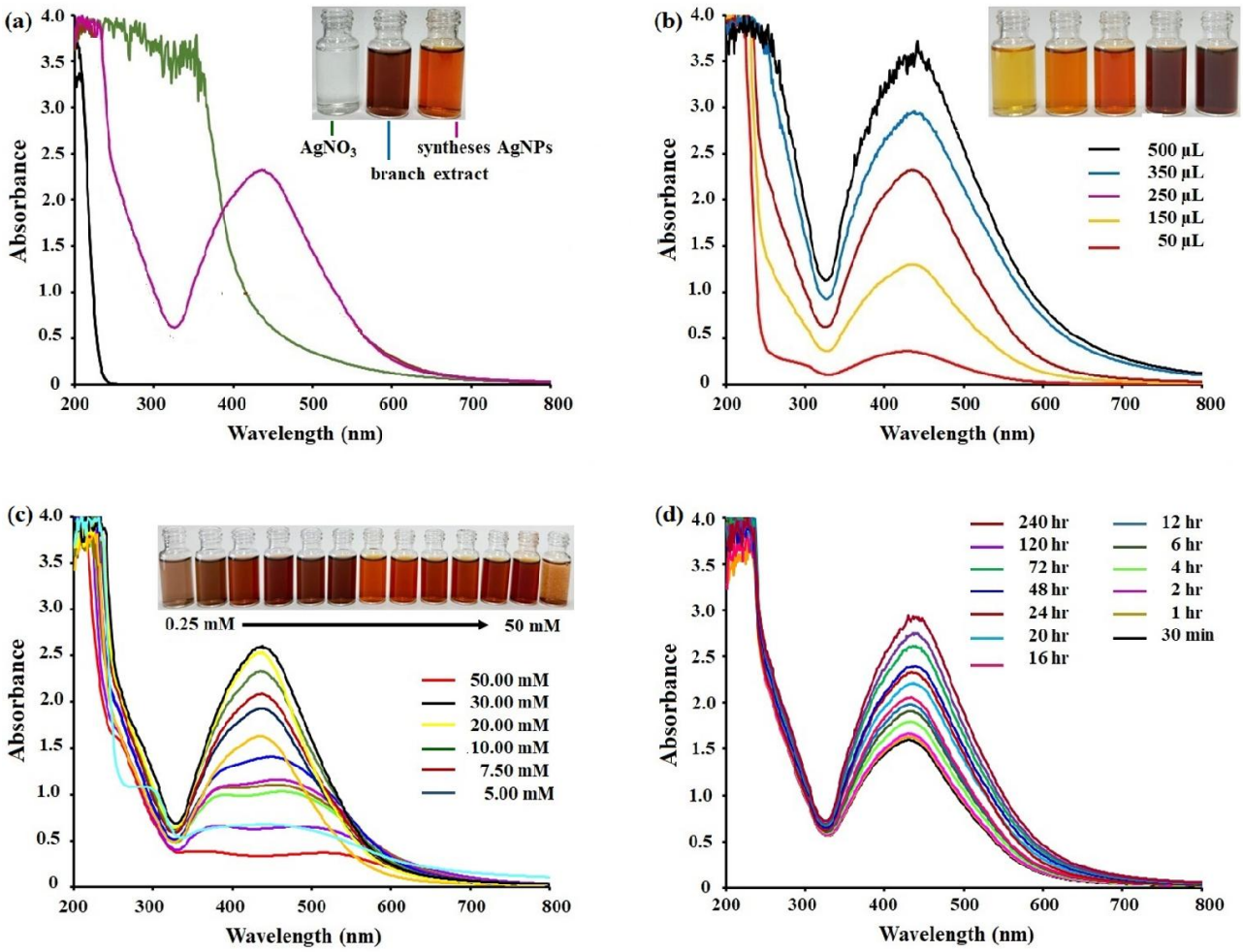


**Figure 1** UV–Vis absorption spectra of silver nanoparticles (AgNPs) synthesized using Syzygium gratum branch extract under controlled reaction conditions. (a) Visual color evolution of the reaction mixture during AgNP formation (inset). (b) Effect of extract volume (50 - 500 µL) on the UV–Vis spectra at a fixed $AgNO_3$ concentration of 10 mM. (c) Effect of $AgNO_3$ concentration (0.25 - 50 mM) at a fixed extract volume of 250 µL. (d) Time-dependent evolution of AgNPs formation monitored by UV–Vis spectroscopy at 10 mM $AgNO_3$ and an extract volume of 250 µL.

The influence of $AgNO_3$ concentration on AgNP synthesis is shown in **Figure 1(c)**. Silver nitrate concentrations ranging from 0.25 to 50 mM were investigated. The concentration of the silver precursor played a crucial role in determining nanoparticle size, stability, and dispersion. At lower concentrations, broad and less intense SPR peaks were observed, suggesting particle agglomeration and the formation of larger nanoparticles. As the $AgNO_3$ concentration increased, the SPR peak became sharper and more intense, indicating improved reduction efficiency and the formation of smaller, more stable nanoparticles. A pronounced SPR peak was observed at 10 mM $AgNO_3$, accompanied by a blue shift from 461 nm to 436 nm, which is indicative of a reduction in nanoparticle size. However, at higher $AgNO_3$ concentrations (> 0.01 M), although monodispersed AgNPs were initially formed, particle aggregation was observed within 5 days, leading to sedimentation. These findings are consistent with previous studies demonstrating that silver precursor concentration critically influences nanoparticle yield, size distribution, and long-term stability. Therefore, 10 mM $AgNO_3$ was selected as the optimal concentration, as it provided well-dispersed and stable AgNPs suitable for antibacterial applications.

The effect of incubation time on AgNPs formation is presented in **Figure 1(d)**. Reaction progress was monitored over incubation periods ranging from 30 min to 240 h. An increase in SPR band intensity with time indicated continuous reduction of $Ag^+$ ions and enhanced nanoparticle formation [45,46]. Within the first 30 min, initial reduction was observed, while a distinct SPR peak at 436 nm appeared after 1 h, confirming the formation of stable AgNPs [47]. The absorbance intensity and color depth continued to increase with prolonged incubation, reaching maximum silver ion reduction after 72 h. This trend can be attributed to an increase in nanoparticle concentration over time [48]. Compared with microbial synthesis routes, which typically require 24 - 124 h [49], the relatively rapid formation of AgNPs in this study highlights the strong reducing capability of *Syzygium gratum* phytochemicals and their effective polymeric stabilization. The reproducibility of the AgNP synthesis was evaluated under identical experimental conditions and performed in triplicate. The resulting SPR absorbance intensity (2.317 ± 0.03) and peak position (436 ± 1 nm) demonstrated excellent reproducibility. This consistency may be attributed to controlled nucleation and growth processes, governed by interactions among high surface-energy nanoparticles and stabilizing biomolecules present in the extract.

**Particle size distribution and zeta potential analysis**

Dynamic light scattering (DLS) was employed to evaluate the hydrodynamic size distribution of AgNPs synthesized using *Syzygium gratum* brance extract. It should be noted that DLS reports the hydrodynamic diameter, which includes the metallic silver core together with the surrounding organic capping layer and solvation shell; consequently, the measured size is typically larger than that obtained from electron microscopy techniques [50]. The DLS results revealed a single dominant peak with a Z-average hydrodynamic diameter of 52.88 nm (**Figure 2(a)**), indicating a relatively narrow size distribution for a biologically synthesized nanoparticle system. The polydispersity index (PDI) was 0.225, which, while not representative of an ideally monodisperse system, lies within the range commonly reported for stable plant-mediated AgNPs [50]. The moderate breadth of the size distribution is attributed to heterogeneous phytochemical capping inherent to biosynthetic routes, reflecting variations in surface-bound biomolecules rather than uncontrolled aggregation.

Zeta-potential measurements further elucidated the colloidal stability of the AgNP suspension (**Figure 2(b)**). The particles exhibited a mean zeta potential of approximately −27.8 mV, accompanied by additional negatively charged subpopulations. Zeta-potential values at or below −27.8 mV are generally considered sufficient to provide electrostatic stabilization through interparticle repulsion in aqueous colloidal systems [51]. The observed surface-charge behavior is consistent with effective adsorption of brance-derived phytochemicals, contributing to colloidal stabilization. Taken together, the combination of moderate hydrodynamic size, acceptable PDI, and sufficiently negative zeta potential supports the conclusion that AgNPs synthesized using *Syzygium gratum* brance extract form a stable colloidal system without the need

for external stabilizers. This stability can be attributed to surface-associated phytochemicals, whose chemical nature and functional features are further discussed in the FT-IR analysis. The results underscore the advantage of woody tissue-derived extracts in providing persistent surface capping and enhanced colloidal stability compared with less stable leaf-derived systems.

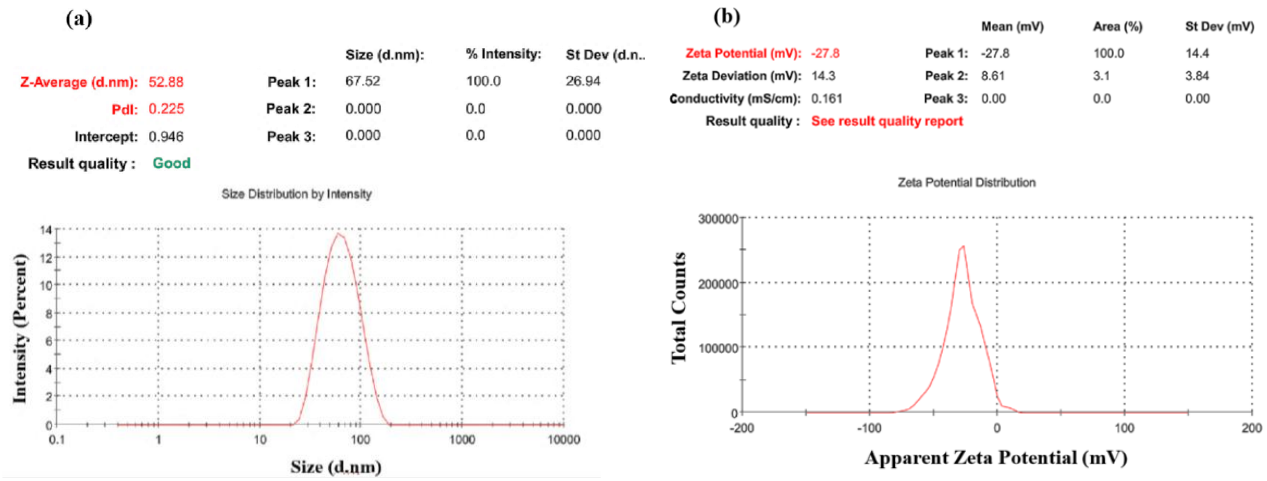


**Figure 2** (a) Dynamic light scattering (DLS) particle size distribution and (b) zeta potential profile of silver nanoparticles (AgNPs) synthesized using *Syzygium gratum* branch extract.

**FT-IR analysis**

FT-IR spectroscopy was employed to identify the functional groups involved in the reduction and stabilization of AgNPs by *Syzygium gratum* branch extract. The FT-IR spectrum of $AgNO_3$ exhibited characteristic absorption bands at 2,729.20, 2,395.20, 1,763.25, and 825.13 $cm^{-1}$ (**Figure 3(a)**), corresponding to nitrate-related vibrational modes. The FT-IR spectrum of the *Syzygium gratum* branch extract (**Figure 3(b)**) showed several prominent peaks, indicating the presence of various bioactive compounds. The band observed at 616.28 $cm^{-1}$ is attributed to alkyl halide vibrations, particularly C–Cl stretching. A distinct peak at 767.29 $cm^{-1}$ corresponds to out-of-plane C–H bending vibrations of alkenes or alkynes. The absorption band at 1,071.22 $cm^{-1}$ is assigned to C–OH stretching vibrations, commonly associated with proteins and polysaccharides. Peaks at 1,238.24 and 1,384.22 $cm^{-1}$ can be attributed to the stretching vibrations of alcohols, ethers, esters, carboxylic acids, and amino groups. The band around 1,381.22 $cm^{-1}$ is related to aromatic C=C stretching vibrations. A prominent peak at approximately 1,612.19 $cm^{-1}$ corresponds to C=O stretching vibrations of carbonyl groups, which may also overlap with amide I or amide II bands of proteins. The absorption bands at 2,930.24 and 3,401.18 $cm^{-1}$ are associated with the stretching vibrations of N–H (secondary amines) and O–H functional groups, respectively. The broad and intense O–H stretching band indicates the presence of hydroxyl groups, suggesting their significant role in the reduction of $Ag^+$ ions and their strong binding affinity toward AgNPs. These hydroxyl groups are most likely attributed to phenolic, alcoholic, and polyphenolic constituents present in the *Syzygium gratum* branch extract, which play a crucial role in the reduction and stabilization of silver ions. This interpretation is in good agreement with previous studies reported by Prakash *et al*. [53] and Wang and Bunkers [54], who similarly identified hydroxyl-rich phytochemicals as key functional groups involved in plant-mediated nanoparticle synthesis.

The FT-IR spectrum of the synthesized AgNPs (**Figure 3(c)**) displayed characteristic peaks at 1,043.05, 1,228.24, 1,612.25, and 2,930.24 $cm^{-1}$, along with several weaker bands. The band at 1,043.05 $cm^{-1}$ is attributed to C–N stretching vibrations of aliphatic amine groups or contributions from phenolic and alcoholic compounds. The peaks at 1,238.24 and 1,612.25 $cm^{-1}$ correspond to amide III and amide II bands of proteins, respectively, while the band at 2,930.24 $cm^{-1}$ is associated with carbonyl groups and secondary amines. The observed shifts and intensity

changes in these functional groups after AgNPs formation indicate that biomolecules present in the branch extract, particularly proteins and polyphenolic compounds, play a crucial role in the reduction and stabilization of AgNPs. The coordination between silver ions and amide nitrogen atoms suggests that proteins act as capping agents, forming a protective layer around the nanoparticles, thereby preventing agglomeration and enhancing colloidal stability. Overall, the FT-IR results confirm that the green synthesis of AgNPs is mediated by plant-derived metabolites, such as terpenoids, proteins, and polyphenols, containing functional groups including amines, alcohols, aldehydes, ketones, and carboxylic acids [55,56].

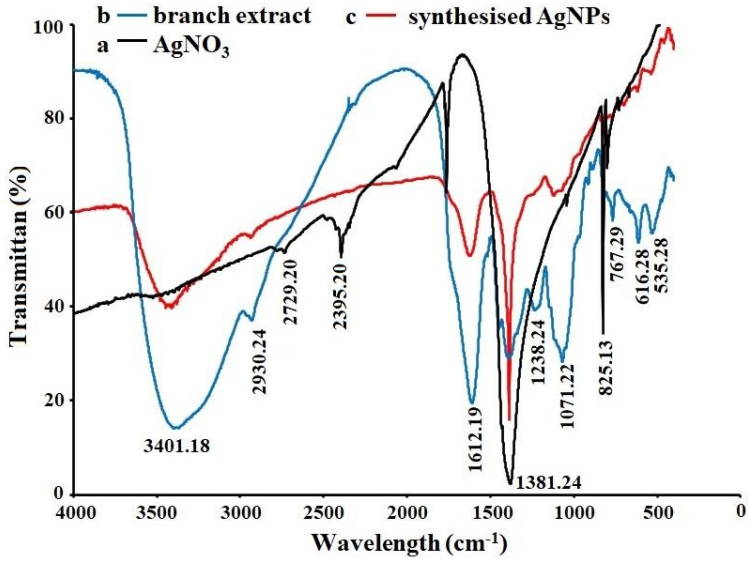


**Figure 3** FTIR spectra of (a) $AgNO_3$, (b) *Syzygium gratum* branch extract, and (c) synthesized silver nanoparticles (AgNPs).

**XRD analysis**

The X-ray diffraction (XRD) pattern of the synthesized AgNPs is shown in **Figure 4**. The presence of sharp and well-defined diffraction peaks confirms the crystalline nature of the nanoparticles. The prominent diffraction peaks observed at 2θ values of 38.15°, 44.32°, 64.47°, and 77.40° correspond to the (111), (200), (220), and (311) crystallographic planes of face-centered cubic (fcc) silver, respectively. These reflections are in good agreement with the standard diffraction data for metallic silver (JCPDS No. 04–0783) [57]. In addition to the characteristic Bragg peaks of silver nanocrystals, minor diffraction peaks at 2θ = 27.19° and 32.24° were also detected. These diffraction peaks can be ascribed to the presence of organic constituents originating from the *Syzygium gratum* branch extract, which actively participate in the reduction of $Ag^+$ ions and subsequently contribute to the stabilization of the synthesized nanoparticles. This observation is consistent with the findings of Konduri *et al*. [58], who reported that phytochemical components from *Hibiscus tiliaceus* leaf extract served as effective reducing and capping agents during the green synthesis of AgNPs. The coexistence of organic-related peaks further substantiates the role of plant-derived biomolecules as natural capping agents in the green synthesis process. Moreover, the sharpness and high intensity of the diffraction peaks reflect a high degree of crystallinity of the AgNPs, in good agreement with earlier reports by Vidhu *et al*. [59], who similarly observed well-defined crystalline structures in biosynthesized silver nanoparticles prepared using plant-based extracts. The average crystallite size of the AgNPs was estimated using the Debye–Scherrer equation, $D = k\lambda/\beta\cos\theta$, where D represents the average crystallite size (Å), *k* is the shape factor (0.9), λ is the X-ray wavelength (1.5406 Å), β denotes the full width at half maximum (FWHM) of the diffraction peak, and θ is the Bragg angle. Based on the (111) diffraction plane, the calculated average crystallite size was 11.65 nm (**Table 1**), which is in close agreement with the average particle size of approximately 11.65 nm. It is

noteworthy that the crystallite size derived from XRD analysis is smaller than the particle size observed in SEM and TEM images. This difference can be attributed to the aggregation of several crystalline domains into larger particles, resulting in an apparent increase in particle size when evaluated by microscopic techniques.

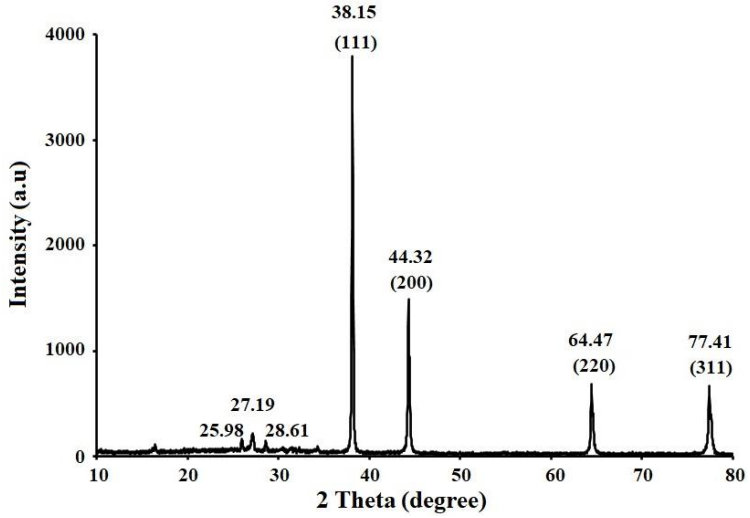


**Figure 4** X-ray diffraction (XRD) pattern of AgNPs synthesized using *Syzygium gratum* branch extract.

**Table 1** Estimated average crystallite size of the synthesized silver nanoparticles calculated using the Debye–Scherrer equation.

| Standard (2θ) JCPDS No:04-8730 | 2θ | θ | sinθ | cosθ | d-spacing [Å] (d = nλ/2sinθ) | B (degree) | FWHM β (radian) | 2sinθ | d (dpacing) | β cosθ | hkl | D (nm) |
|---|---|---|---|---|---|---|---|---|---|---|---|---|
| 38.117 | 38.154 | 19.077 | 0.764 | 0.945 | 2.357 | 0.561 | 0.010 | 0.653 | 0.236 | 0.0090 | (111) | 15.645 |
| 44.279 | 44.328 | 22.191 | 0.376 | 0.926 | 2.042 | 1.461 | 0.025 | 0.7529 | 0.205 | 0.0240 | (200) | 6.1310 |
| 64.428 | 64.471 | 32.235 | 0.532 | 0.845 | 1.444 | 0.718 | 0.012 | 1.0675 | 0.144 | 0.0106 | (220) | 13.667 |
| 77.475 | 77.415 | 38.707 | 0.625 | 0.780 | 1.232 | 0.955 | 0.017 | 1.0251 | 0.123 | 0.0130 | (311) | 11.136 |

**SEM and EDX analysis**

The surface morphology of the synthesized AgNPs was examined by scanning electron microscopy (SEM), as shown in **Figures 5(a) - 5(b)**. Discrete nanoscale features with predominantly irregular to quasi-spherical appearances were observed, distributed across the substrate. A certain degree of particle clustering was evident, which is commonly attributed to solvent evaporation and sample dehydration during SEM preparation rather than intrinsic colloidal instability [60]. As SEM provides localized surface information, the apparent particle dimensions observed in the micrographs should be interpreted qualitatively and in conjunction with size information obtained from TEM and DLS analyses.

The elemental composition of the synthesized material was further examined by SEM–EDS (**Figure 5(c)**). The EDS spectrum displayed a prominent signal corresponding to elemental silver, confirming Ag as the dominant inorganic constituent of the synthesized nanoparticles. This characteristic silver peak is in good agreement with previously reported EDS profiles of biosynthesized AgNPs [61]. In addition, detectable carbon and oxygen signals were observed, which can be attributed to organic moieties derived from the *Syzygium gratum* branch extract. Similar elemental contributions from plant-based biomolecules acting as reducing and capping agents have been reported by Jyoti *et al*. [60] in their study on *Urtica dioica*–mediated silver nanoparticle synthesis, further supporting the involvement of phytochemical constituents in the stabilization of the AgNPs. In addition, carbon and oxygen signals were detected, which are associated with organic species originating from the Syzygium gratum

branch extract. These surface-associated organic components are consistent with phytochemical capping inferred from FT-IR and zeta-potential analyses and support their role in stabilizing the AgNPs within an organic matrix. The SEM–EDS results therefore provide complementary evidence for the formation of silver nanoparticles embedded in a phytochemically derived surface environment, in agreement with the physicochemical characteristics discussed in the preceding sections.

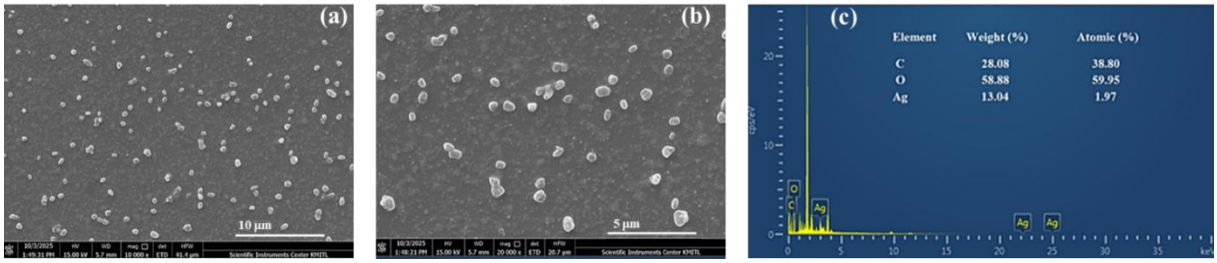


**Figure 5** (a) - (b) SEM images, and (c) EDX spectrum of AgNPs synthesized using *Syzygium gratum* branch extract.

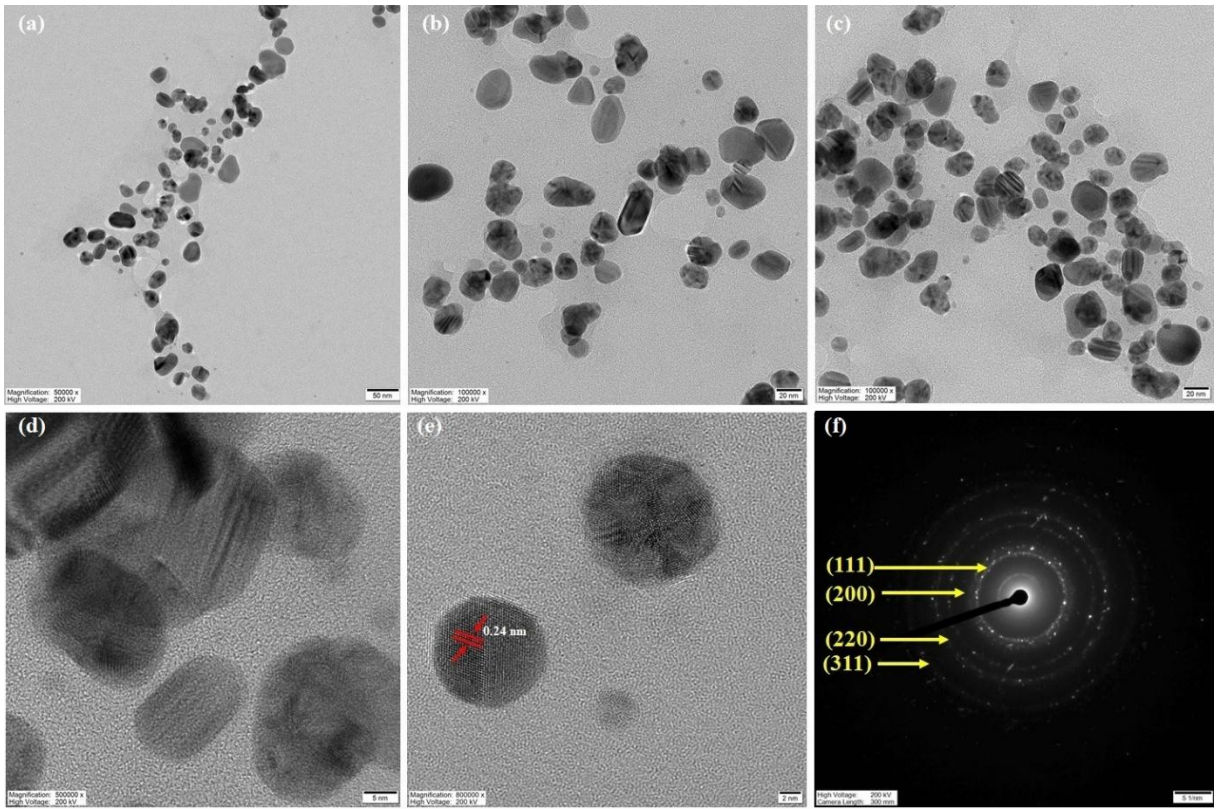


**Figure 6** (a) - (d) HRTEM micrographs, (e) lattice fringes at higher magnification, and (f) SAED pattern of AgNPs synthesized using *Syzygium gratum* branch extract.

**HRTEM and SAED analysis**

HRTEM analysis was employed to further elucidate the surface morphology, shape, and particle size distribution of the synthesized AgNPs. Representative HRTEM micrographs are shown in **Figures 6(a) - 6(e)**. The AgNPs exhibited diverse morphologies, including spherical, triangular, hexagonal, and rod-like structures, with smooth surface features. Statistical analysis based on TEM images of more than 100 individual nanoparticles revealed particle diameters ranging from approximately 2 to 50 nm, with an average particle size of 92.88 ± 11.17 nm. The corresponding particle size distribution histogram (**Figure 6(g)**) indicates a moderately narrow size distribution, confirming the effective size control achieved through the phytochemical-mediated

reduction and stabilization process. The nanoparticles were well dispersed with minimal aggregation at the nanoscale, suggesting efficient surface capping by biomolecules present in the *Syzygium gratum* branch extract. The selected area electron diffraction (SAED) pattern shown in **Figure 6(f)** displayed distinct concentric rings, confirming the polycrystalline nature of the AgNPs. These diffraction rings were indexed to the (111), (200), (220), and (311) crystallographic planes, which are characteristic reflections of the face-centered cubic (FCC) structure of metallic silver. The SAED results further corroborate the high crystallinity of the biosynthesized AgNPs.

**Antibacterial activity**

The antibacterial activity of the synthesized AgNPs was evaluated against six representative bacterial strains, namely *E. coli*, *P. aeruginosa*, *S. aureus*, *L. monocytogenes*, *S. typhimurium*, and *B. cereus* using the disk diffusion method. The biosynthesized AgNPs exhibited pronounced antibacterial activity against all tested bacterial strains. The measured zones of inhibition (ZOIs) are summarized in **Table 2** and illustrated in **Figure 7**. Statistical analysis revealed that the antibacterial effects of the AgNPs were significant ($p < 0.05$) for five of the six tested bacterial species, indicating a strong likelihood that the observed inhibition was attributable to the nanoparticles. Although *L. monocytogenes* showed a relatively large inhibition zone, the difference was not statistically significant ($p = 0.061$). Such variations in antibacterial susceptibility can be attributed to differences in bacterial species, cell wall architecture, nanoparticle concentration, and experimental conditions. In particular, Li *et al*. [61] demonstrated that the antibacterial efficacy of AgNPs against multidrug-resistant *Pseudomonas aeruginosa* is strongly influenced by bacterial membrane structure and nanoparticle–cell interactions, which govern membrane disruption and intracellular damage. The magnitude of antibacterial activity, expressed as effect size, serves as a quantitative indicator of efficacy, with larger values reflecting stronger bactericidal performance. Consistent with this, previous studies have reported that AgNPs exhibit large effect sizes (Cohen's d = 1.08 - 4.29), primarily due to their nanoscale dimensions and high surface-area-to-volume ratio, which enhance direct contact with bacterial membranes and promote $Ag^+$ ion release. This interpretation is in good agreement with the findings of Ershov and Ershov [62], who reported a strong size-dependent relationship between silver nanoparticles and antibacterial activity, highlighting the superior bactericidal performance of smaller AgNPs.

The antibacterial activity of the green-synthesized AgNPs exhibited a clear concentration-dependent enhancement, in good agreement with previously reported studies [63]. Notably, at an AgNPs concentration corresponding to 10 mM $AgNO_3$, the largest zones of inhibition (ZOIs) were observed, measuring 18.67 ± 0.58 mm for *P. aeruginosa*, 14.33 ± 1.53 mm for *L. monocytogenes*, 12.67 ± 1.15 mm for *E. coli*, 15.33 ± 1.15 mm for *S. aureus*, 13.33 ± 0.58 mm for *S. typhimurium*, and 15.00 ± 1.00 mm for *B. cereus*. This pronounced antibacterial performance can be attributed to the increased availability of AgNPs at higher concentrations, which enhances nanoparticle–bacteria interactions and $Ag^+$ ion release. Similar concentration-dependent antibacterial and antibiofilm effects of AgNPs against both Gram-positive and Gram-negative bacteria were reported by Gurunathan *et al*. [63], who highlighted membrane disruption and intracellular oxidative stress as key mechanisms underlying AgNP-induced bacterial inhibition. In contrast, the *Syzygium gratum* branch extract alone exhibited comparatively weaker antibacterial activity, yielding ZOIs of 9.67 ± 0.58 mm against *P. aeruginosa* and 7.67 ± 0.58 mm against *B. cereus*, suggesting a limited intrinsic antimicrobial effect of the phytochemicals in the absence of nanoparticle formation. The $AgNO_3$ solution produced moderate inhibition zones ranging from 9.33 to 13.67 mm across all tested strains, indicating that the enhanced antibacterial efficacy observed for the AgNPs arises from the synergistic effects of nanoscale silver and plant-derived capping agents rather than from ionic silver alone.

Overall, the biosynthesized AgNPs demonstrated markedly higher antibacterial activity, yielding inhibition zones of approximately 13 - 19 mm, compared with $AgNO_3$ (9 - 14 mm) and the crude plant extract (7 - 10 mm). This enhanced bactericidal performance can be attributed to the extremely large surface area of AgNPs, which promotes close contact with microbial cells and acts as a reservoir for sustained

$Ag^+$ ion release. Slight variations in antibacterial efficacy among bacterial species are likely related to differences in cell wall architecture, surface charge, nanoparticle size, intracellular targets, resistance mechanisms, and potential synergistic interactions with phytochemicals present on the nanoparticle surface. The antibacterial mechanism of AgNPs involves multiple pathways. Initially, AgNPs interact with bacterial cell membranes, disrupting membrane integrity, permeability, and respiratory functions. Subsequently, AgNPs can penetrate the cell envelope and enter the cytoplasm, where they interact with sulfur-containing proteins and phosphorus-rich biomolecules such as DNA and RNA, ultimately leading to cell death. Silver nanoparticles exhibit a strong affinity for sulfur and phosphorus, elements abundant in both Gram-positive and Gram-negative bacterial membranes. Binding of AgNPs to thiol-containing proteins significantly reduces bacterial viability. In addition, internalized AgNPs can interfere with intracellular signaling pathways, metabolic processes, DNA replication, cellular respiration, and cell division, culminating in extensive bacterial damage and loss of viability [64-66].

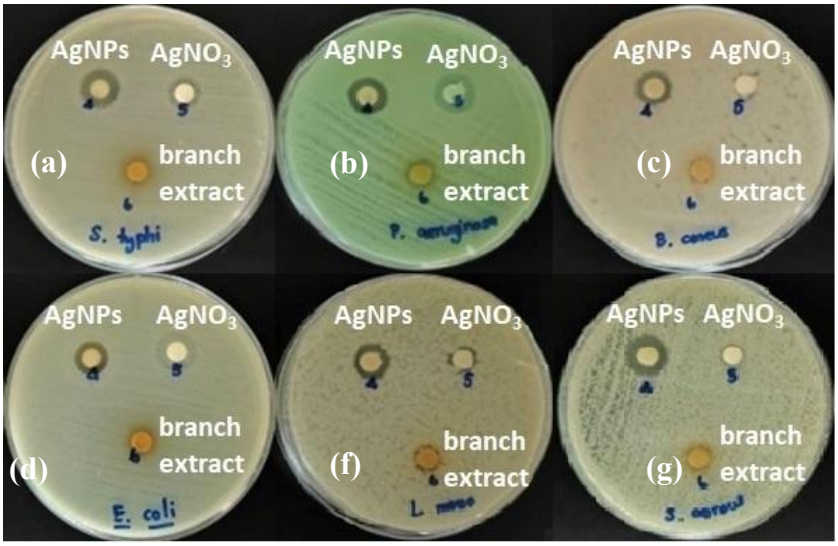


**Figure 7** Antibacterial activity of biosynthesized AgNPs against six bacterial strains as determined by the disk diffusion method: (a) *S. typhimurium*, (b) *P. aeruginosa*, (c) *B. cereus*, (d) *E. coli*, (e) *L. monocytogenes*, and (f) *S. aureus*.

**Table 2** Antibacterial performance of silver nanoparticles synthesized via a green route using *Syzygium gratum* branch extract against selected bacterial strains.

| Microorganisms | Diameter of inhibition zone (mm) | | | Estimated | | |
|---|---|---|---|---|---|---|
| | branch extract | $AgNO_3$ | AgNPs | *p*-value | Cohen's *d* | Interpretation |
| *Escherichia coli* | NS | 9.33 ± 1.53[a] | 12.67 ± 1.15[a] | 0.032 | 2.31[c] | Large effect, significant ($p < 0.05$) |
| *Pseudomonas aeruginosa* | 9.67 ± 0.58[a] | 12.00 ± 2.00[a] | 18.67 ± 0.58[a] | 0.008 | 4.29[c] | Large effect, significant ($p < 0.05$) |
| *Staphylococcus aureus* | NS[b] | 13.67 ± 1.53[a] | 15.33 ± 1.15[a] | 0.049 | 1.23[c] | Large effect, significant ($p < 0.05$) |
| *Listeria monocytogenes* | NS[b] | 12.00 ± 1.00[a] | 14.33 ± 1.53[a] | 0.061 | 1.08[c] | Large effect, not significant ($p < 0.05$) |
| *Salmonella typhimurium* | NS[b] | 10.67 ± 0.58[a] | 13.33 ± 0.58[a] | 0.039 | 1.35[c] | Large effect, significant ($p < 0.05$) |
| *Bacillus cereus* | 7.67 ± 0.58[a] | 11.33 ± 1.15[a] | 15.00 ± 1.00[a] | 0.021 | 2.01[c] | Significant difference ($p < 0.05$) |

Noted: [a] Each value is an average of three replicates ± standard deviation (SD).

[b] NS = non-sensitive

[c] Cohen's *d* is a measure of effect size that quantifies the difference between two means in terms of standard deviations.

## Conclusions

A green A green and reproducible approach for the synthesis of silver nanoparticles was successfully developed using *Syzygium gratum* branch extract as a dual-function reducing and stabilizing agent. Systematic optimization of the reaction parameters, including $AgNO_3$ concentration, extract volume, and incubation time, enabled controlled nanoparticle formation. Comprehensive physicochemical characterization using UV–Vis spectroscopy, FTIR, XRD, SEM, HRTEM, EDX, and zeta-potential analyses confirmed the successful synthesis of well-defined AgNPs. The biosynthesized AgNPs exhibited a characteristic surface plasmon resonance band centered at 436 nm and a face-centered cubic crystalline structure, with an average crystallite size of 11.65 nm, confirming effective reduction and crystallization under mild, plant-mediated conditions. The pronounced negative zeta potential indicated good colloidal stability, while electron microscopy analyses revealed nanoscale particles with well-dispersed morphology and size heterogeneity associated with the phytochemical environment of woody tissue extracts. FT-IR analysis suggested that phytochemical functional groups, particularly hydroxyl- and amide-containing compounds, played a key role in the reduction of $Ag^+$ ions and in nanoparticle surface capping, thereby contributing to structural stability and dispersion. Importantly, the AgNPs synthesized using branch-derived extract demonstrated notable antibacterial activity against both Gram-positive and Gram-negative bacterial strains, highlighting the strong bio–nano interfacial interactions induced by surface-bound phytochemicals.

Overall, this study provides new insight into how woody-tissue-derived phytochemical matrices influence nanoparticle nucleation, growth behavior, surface chemistry, and antibacterial performance, rather than focusing solely on synthesis optimization. Future work will focus on correlating specific surface-bound phytochemicals with antibacterial mechanisms, evaluating cytotoxicity and biocompatibility for biomedical relevance, and exploring the integration of these AgNPs into functional coatings, filtration media, or antimicrobial composites. Despite the advantages of the proposed green synthesis approach, certain limitations should be acknowledged for large-scale implementation. Variability in phytochemical composition arising from plant age, seasonal factors, and extraction conditions may influence nanoparticle reproducibility and batch-to-batch consistency. In addition, precise control over particle size distribution and morphology during scale-up remains a challenge that requires further process optimization. Future studies should therefore address scalable reactor design, standardization of extract preparation, and continuous-flow synthesis strategies to ensure reproducibility and cost-effectiveness for industrial applications. The environmentally benign synthesis strategy presented here offers a scalable and sustainable route for producing functional silver nanomaterials, with potential relevance for antimicrobial and biointerface-related applications.

## Acknowledgements

The authors gratefully acknowledge the financial support provided by the National Research Council of Thailand. The authors also thank the Department of Chemistry, Faculty of Science and Technology, Rajabhat Rajanagarindra University, for providing laboratory facilities.

## Declaration of generative AI in scientific writing

During the preparation of this manuscript, the authors employed AI-assisted tools, including Google-based services and ChatGPT (OpenAI), exclusively to improve linguistic clarity and correct grammatical issues. These tools were not used for generating scientific content, performing data analysis, or interpreting experimental results. The authors retain complete responsibility for the originality, accuracy, and scientific integrity of the work reported herein.

## CRediT author statement

**Amornrassamee Jinnarak**: Conceptualization; Methodology; Investigation; Formal analysis; Data Curation; Investigation; Writing - Original Draft; Writing - Review & Editing. **Taweesub Juepanit**: Conceptualization; Methodology; Investigation; Formal analysis; Data Curation. **Nichanun Udomsaksakul**: Conceptualization; Methodology; Investigation; Formal analysis; Data Curation. **Wuttichai Roschat**: Conceptualization; Formal analysis; Data Curation;

Investigation; Supervision; Writing - Review & Editing. **Phakawan Kongchantree**: Conceptualization; Methodology; Investigation; Formal analysis; Data Curation; Investigation; Writing - Original Draft; Writing - Review & Editing.

**References**


[1] Z Wu, W Deng, J Luo and D Deng. Multifunctional nano-cellulose composite films with grape seed extracts and immobilized silver nanoparticles. *Carbohydrate Polymers* 2019; **205**, 447-455.

[2] KK Kadhim, HM Azeez, RT Yousif, MK Mohammed and MH Meteab. Boosting the structural, optical and AC electrical characteristics of PVA/CdTe nanocomposites for flexible smart optoelectronic devices. *International Journal of Nanoelectronics and Materials* 2025; **18(4)**, 527-536.

[3] HK Obayes, MH Meteab and B Abd Al-Kareem. Modified dosimetric features of a new type of lithium borate glass system: Role of magnesium and gold co-doping. *Transactions on Electrical and Electronic Materials* 2024; **25**, 708-721.

[4] AN Hadi, MH Meteab and MK Mohammed. Influence of inclusion $Sb_2O_3$/NiO nanostructures on the morphological, microstructural, and optical characteristics of PVA polymeric for gamma-ray shielding applications. *Revue des Composites et des Matériaux Avancés – Journal of Composite and Advanced Materials* 2025; **35(3)**, 581-591.

[5] MJ Madiabu, I Solihat, DAN Widyahapsari, H Rochaeni, AM Ichzan, DOB Apriandanu, R Rahman, N Sugiarto, R Nur and H Rahmawati. Plant-mediated silver nanoparticles derived from *Dioscorea hispida* and evaluation of their antioxidant, antibacterial ability, and $Hg^{2+}$ detection activities. *Next Materials* 2025; **8**, 100858.

[6] RA Alzahrani, FG Alhaddad, EO Alshammari, FS Alsowaileh, MD Alghamdi, A Modwi, AM Almehmadi and M Alanazi. Silver nanoparticles in gas sensing: A comprehensive review of synthesis mechanisms, performance metrics, and emerging applications. *Journal of Science: Advanced Materials and Devices* 2025; **10(3)**, 100964.

[7] S Ghosh and SN Sinha. Untying the antimicrobial and antioxidant potential of silver nanoparticles fabricated from *Typhonium trilobatum* (L.) Schott. *Plant Nano Biology* 2024; **10**, 100113.

[8] L Muthulakshmi, K Suganya, M Murugan, J Annaraj, V Duraipandiyan, A Duni and A Alharbi. Antibiofilm efficacy of novel biogenic silver nanoparticles from *Terminalia catappa* against food-borne *Listeria monocytogenes* ATCC 15313. *Journal of King Saud University - Science* 2022; **24**, 102083.

[9] H Jan, G Zaman, H Usman, R Ansir, S Drouet, N Gigliolo-Guivarc'h, S Kousar and S Shah. Biogenically proficient synthesis and characterization of silver nanoparticles employing aqueous extract of *Aquilegia pubiflora*. *Journal of Materials Research and Technology* 2021; **15**, 950-968.

[10] O Bondarenko, K Juganson, A Ivask, K Kasemets, M Mortimer and A Kahru. Toxicity of Ag, CuO and ZnO nanoparticles to environmentally relevant organisms and mammalian cells. *Archives of Toxicology* 2013; **87**, 1181-1200.

[11] V Priyadarshini, K Tharini, G Kalaimagal, AA Kalicharan, B Subhashini, A Rathinavelu and S Mohan. Green engineered silver nanoparticles enabling thermal, optical and catalytic behavior. *Results in Surfaces and Interfaces* 2025; **20**, 100593.

[12] H Ahmed, MY Zaky, MMA Rashed, M Almoiliqy, S Al-Dalali, ZE Eldin, M Moustafa, A Ibrahim, M Al-Haj and A Al-Gheethi. UPLC-qTOF-MS phytochemical profiling and synthesis of silver nanoparticles for enhanced antibacterial activity. *Ultrasonics Sonochemistry* 2024; **107**, 106923.

[13] SR Devi and B Dhurai. Synthesis of silver nanoparticles using *Pongamia pinnata* leaf extract for dye removal under solar irradiation. *Desalination and Water Treatment* 2023; **315**, 373-386.

[14] S Sivakami, V Thangapushbam, P Rama, M Jothika, R Sundaram, N Arumugam and A Perumal. Green synthesis of silver nanoparticles from *Muntingia calabura* fruit extract. *Chemical Inorganic Materials* 2025; **7**, 100112.

[15] J Wang, Z Wang, J Yun, S Chen, S Liu, C Li and Y Sun. Ball milling-induced disassembly of cellulose in coconut endosperm pomace. *International Journal of Biological Macromolecules* 2025; **310**, 143238.

[16] C Qian, X Dong, HS Althaf, L Wang and G Zhao. Green-formulated silver nanoparticles for hydrazine sensing and breast cancer treatment. *Journal of Science: Advanced Materials and Devices* 2024; **9**, 100691.

[17] D Singha, N Barman and K Sahu. Facile synthesis of high-optical-quality silver nanoparticles by ascorbic-acid reduction. *Journal of Colloid and Interface Science* 2014; **413**, 37-42.

[18] E Charistoudi, MG Kallitsakis, I Charisteidis, KS Triantafyllidis and IN Lykakis. Selective reduction of azines catalyzed by silver nanoparticles. *Advanced Synthesis & Catalysis* 2017; **359**, 2949-2960.

[19] A Fahrina, N Arahman, MR Bilad, S Aprilia, A Mulyati, BY Gül, R Putra and M Nasrullah. High-performance antibacterial composite membrane with silver nanoparticles. *South African Journal of Chemical Engineering* 2024; **40**, 404-414.

[20] S Rajeshkumar and LV Bharath. Mechanism of plant-mediated synthesis of silver nanoparticles. *Chemico-Biological Interactions* 2017; **273**, 219-227.

[21] P Singh, YJ Kim, D Singh, H Choi, S Yang, J Mathiyalagan, S Kumar and DC Yang. Biosynthesis, characterization, and antimicrobial applications of silver nanoparticles using *Panax ginseng* root extract. *Colloids and Surfaces B: Biointerfaces* 2015; **133**, 284-290.

[22] S Iravani, H Korbekandi, SV Mirmohammadi and B Zolfaghari. Synthesis of silver nanoparticles: Chemical, physical and biological methods. *Research in Pharmaceutical Sciences* 2014; **9**, 385-406.

[23] NA Sami, AM Nattah, RA Jawad, MH Meteab and MK Mohammed. Modification and enhancement of the structural, morphological, and optical characteristics of PMMA/$In_2O_3$/$SiO_2$ promising ternary nanostructures for optical nanodevices and gamma-ray attenuation. *Trends in Sciences* 2025; **22(7)**, 9959.

[24] M Vanaja, G Gnanajobitha, K Paulkumar, S Rajeshkumar, C Malarkodi and G Annadurai. Phytosynthesis of silver nanoparticles by *Cissus quadrangularis*: Influence of physicochemical factors. *Journal of Nanostructure in Chemistry* 2013; **3**, 17.

[25] M Dipankar and S Murugan. Green synthesis, characterization and biological activities of silver nanoparticles synthesized from *Iresine herbstii* leaf aqueous extract. *Colloids and Surfaces B: Biointerfaces* 2012; **98**, 112-119.

[26] AK Mittal, Y Chisti and UC Banerjee. Synthesis of metallic nanoparticles using plant extracts. *Biotechnology Advances* 2013; **31**, 346-356.

[27] S Chotchoungchatchai, P Saralamp, T Jenjittikul, S Pornsiripongse and S Prathanturarug. Medicinal plants used with Thai Traditional Medicine in modern healthcare services: A case study in Kabchoeng Hospital, Surin Province, Thailand. *Journal of Ethnopharmacology* 2012; **141**, 193-205.

[28] WK Soh and J Parnell. A revision of *Syzygium* Gaertn. (Myrtaceae) in Indochina (Cambodia, Laos and Vietnam). *Adansonia* 2015; **37(2)**, 179-275.

[29] G Rocchetti, L Lucini, SR Ahmed and FR Saber. *In vitro* cytotoxic activity of six *Syzygium* leaf extracts as related to their phenolic profiles: An untargeted UHPLC-QTOF-MS approach. *Food Research International* 2019; **126**, 108715.

[30] DK Saini, M Singh, JK Pandey, S Rathore, RP Singh and M Kumar. Green synthesis of nanoparticles for biomedical applications. *Journal of Materials and Environmental Science* 2025; **16(10)**, 1833-1859.

[31] Y Bao, J He, K Song, J Guo, X Zhou and S Liu. Plant-extract-mediated synthesis of metal nanoparticles. *Journal of Chemistry* 2021. https://doi.org/10.1155/2021/6562687

[32] D Tripathi, A Modi, G Narayan and SP Rai. Green and cost-effective synthesis of silver nanoparticles from endangered medicinal plant Withania coagulans and their biomedical potential. *Materials Science and Engineering C* 2019; **100**, 152-164.

[33] DK Bhui, H Bar, P Sarkar, GP Sahoo, SP De and A Misra. Synthesis and UV–vis spectroscopic

study of silver nanoparticles in aqueous SDS solution. *Journal of Molecular Liquids* 2009; **145**, 33-37.

[34] Y Sun, SK Gray and S Peng. Surface chemistry as a critical parameter determining optical properties of small colloidal metal nanoparticles. *Physical Chemistry Chemical Physics* 2011; **13**, 11814-11826.

[35] N Pugazhenthiran, S Murugesan, T Muneeswaran, S Suresh, M Kandasamy, H Valdés, M Selvaraj, AD Savariraj and RV Mangalaraja. Biocidal activity of *Citrus limetta* peel extract-mediated silver quantum dots against MCF-7 cells and pathogenic bacteria. *Journal of Environmental Chemical Engineering* 2021; **9**, 105089.

[36] L Sintubin, DWD Windt, J Dick, J Mast, DV Ha, W Verstraete and N Boon. Lactic acid bacteria as reducing and capping agents for efficient silver nanoparticle production. *Applied Microbiology and Biotechnology* 2009; **84**, 741-749.

[37] MA Ebrahimzadeh, A Naghizadeh, O Amiri, AM Shirzadi and DS Mortazavi. Green synthesis of silver nanoparticles using *Crataegus pentagyna* fruit extract for dye degradation and antibacterial applications. *Bioorganic Chemistry* 2020; **94**, 103425.

[38] A Bazrgaran, S Mahmoodabadi, A Ghasempour, E Shafaie, A Sahebkar and S Eghbali. Biogenic synthesis of *Astragalus sarcocolla* gum extract-mediated silver nanoparticles and their biological activities. *Plant Nano Biology* 2023; **6**, 100052.

[39] S Priyadarshini, S Sulava, R Bhol and S Jena. Green synthesis of silver nanoparticles using *Azadirachta indica* and *Ocimum sanctum* leaf extracts. *Current Science* 2019; **117**, 1300-1307.

[40] A Rahman, G Rehman, N Shah, M Hamayun, S Ali, A Ali, SK Shah, W Khan, MIA Shah and AF Alrefaei. Biosynthesis of silver nanoparticles using *Tribulus terrestris* seeds and their antidiabetic potential. *Molecules* 2023; **28**, 4203.

[41] BM Abegaz and T Kebede. Geshoidin: a bitter principle of *Rhamnus prinoides* and other leaf constituents. *Bulletin of the Chemical Society of Ethiopia* 1995; **9**, 107-114.

[42] IJ Fernandes, AF Aroche, A Schuck, P Lamberty, CR Peter and W Hasenkamp. Silver nanoparticle conductive inks for inkjet-printed flexible electrodes. *Scientific Reports* 2020; **10**, 8878.

[43] O Pryshchepa, P Pomastowski and B Buszewski. Silver nanoparticles: Synthesis, investigation techniques and properties. *Advances in Colloid and Interface Science* 2020; **284**, 102246.

[44] AK Biswal and PK Misra. Biosynthesis and characterization of silver nanoparticles for food packaging and biomedical applications. *Materials Chemistry and Physics* 2020; **250**, 123014.

[45] K Chulasak, C Punsawad and P Rattanakit. Silver nanoparticles synthesized from *Launaea sarmentosa* extract: Synthesis, characterization and antimalarial activity. *Nanotechnology for Environmental Engineering* 2022; **7**, 491-501.

[46] M Chandhru, R Logesh, SK Rani, N Ahmed and N Vasimalai. One-pot green synthesis of silver nanoparticles from jackfruit seeds and their antibacterial activity against *Escherichia coli* and *Salmonella*. *Biocatalysis and Agricultural Biotechnology* 2019; **20**, 101241.

[47] S Shankar, J Chorachoo, L Jaiswal and SP Voravuthikunchai. Effect of reducing-agent concentration and temperature on the characteristics and antimicrobial activity of silver nanoparticles. *Materials Letters* 2014; **137**, 160-163.

[48] KC Bhainsa and SF D'Souza. Extracellular biosynthesis of silver nanoparticles using the fungus *Aspergillus fumigatus*. *Colloids and Surfaces B: Biointerfaces* 2006; **47**, 160-164.

[49] H Korbekandi, S Iravani and S Abbasi. Production of nanoparticles using organisms. *Critical Reviews in Biotechnology* 2009; **29**, 279-306.

[50] LDC Vera-Nuñez, JO Cornejo-Ruiz, CA Arenas-Chávez, LMD Hollanda, A Alvarez-Risco, S Del-Aguila-Arcentales, F Yáñez-Cruz and M Rojas. Green synthesis of silver nanoparticles conjugated with *Thelypteris glandulosolanosa*: Characterization and anticancer activity. *Processes* 2022; **10**, 1308.

[51] RR Remya, SR Rajasree, L Aranganathan and TY Suman. Cytotoxic effects of bioactive silver nanoparticles synthesized using *Cassia fistula* flower extract on MCF-7 breast cancer cells. *Biotechnology Reports* 2015; **10**, 110-115.

[52] S Nagaraja, SS Ahmed, DR Bharathi, P Goudanavar, MR Kumar, S Fattepur, B Naresh and A Gururaj. Green synthesis of silver nanoparticles using *Psidium guajava* leaf extract and evaluation of antidiabetic activity. *Molecules* 2022; **27(14)**, 4336.

[53] P Prakash, P Gnanaprakasam, R Emmanuel, S Arokiyaraj and M Saravanan. Green synthesis of silver nanoparticles from *Mimusops elengi* leaf extract for enhanced antibacterial activity against multidrug-resistant pathogens. *Colloids and Surfaces B: Biointerfaces* 2013; **108**, 255-259.

[54] X Wang and GJ Bunkers. Potent heterologous antifungal proteins from cheeseweed (*Malva parviflora*). *Biochemical and Biophysical Research Communications* 2000; **279(2)**, 669-673.

[55] T Rebecca, F Fenali, L Parvathi and F Glory. Antibacterial and antifungal activity of silver nanoparticles synthesized using *Artocarpus heterophyllus* leaf extract. *Biotechnology, Bioinformatics and Bioengineering* 2012; **2021(21)**, 632-637.

[56] AK Mittal, Y Chisti and UC Banerjee. Synthesis of metallic nanoparticles using plant extracts. *Biotechnology Advances* 2013; **31(2)**, 346-356.

[57] Z Zarei, D Razmjoue, F Oroojalian, M Moazeni and H Azarnivand. *Salvia sclarea* flower extract-mediated green synthesis of silver nanoparticles and their antimicrobial and scolicidal activities. *The Microbe* 2024; **5**, 100216.

[58] VV Konduri, NK Kalagatur, L Gunti, UK Mangamuri, VR Kalagadda, S Poda, B Kamarapu and R Pamanji. Green synthesis of silver nanoparticles using *Hibiscus tiliaceus* leaves and their multifunctional applications. *South African Journal of Botany* 2024; **168**, 476-487.

[59] VK Vidhu, SA Aromal and D Philip. Green synthesis of silver nanoparticles using *Macrotyloma uniflorum*. *Spectrochimica Acta Part A: Molecular and Biomolecular Spectroscopy* 2011; **83**, 392-397.

[60] K Jyoti, M Baunthiyal and A Singh. Characterization of silver nanoparticles synthesized using *Urtica dioica* leaves and their synergistic effects with antibiotics. *Journal of Radiation Research and Applied Sciences* 2016; **9(3)**, 217-227.

[61] S Liao, Y Zhang, X Pan, F Zhu, C Jiang, Q Liu, Z Cheng, G Dai, G Wu, L Wang and L Chen. Antibacterial activity and mechanism of silver nanoparticles against multidrug-resistant *Pseudomonas aeruginosa*. *International Journal of Nanomedicine* 2019; **14**, 1469-1487.

[62] VA Ershov and BG Ershov. Effect of silver nanoparticle size on antibacterial activity. *Toxics* 2024; **12(11)**, 801.

[63] S Gurunathan, JW Han, D Kwon and JH Kim. Enhanced antibacterial and antibiofilm activities of silver nanoparticles against Gram-positive and Gram-negative bacteria. *Nanoscale Research Letters* 2014; **9(1)**, 373.

[64] M Moradialvand, N Asri, M Jahdkaran, M Beladi and H Houri. Advances in nanoparticle-based strategies for enhanced antibacterial interventions. *Cell Biochemistry and Biophysics* 2024; **82**, 3071-3090.

[65] P Phatai, S Siri-Udom, P Khemthong, S Youngjan, T Butburee, W Roschat, R Khunphonoie, CM Futalan, S Kamonwannasit, K Prasitnok and O Prasitnok. Enhanced antibacterial activity of ZIF-8- and ZIF-67-loaded $Mn_{0.5}/Ce_{0.5}$ mixed oxide–hydroxyapatite composites. *Materials Chemistry and Physics* 2025; **346**, 131344.

[66] S Siri-Udom, O Prasitnok, K Prasitnok, P Khemthong, C Phawa, W Roschat, S Utara, N Prachumrak, J Sripirom and P Phatai. Synthesis, characterization, and functional analysis of mixed manganese/cerium oxide/hydroxyapatite nanocomposites for antibacterial applications. *Journal of Cluster Science* 2025; **36**, 28.